CrossMark

Interdiffusion in the Ni-Re System: Evaluation of Uncertainties

W. J. Boettinger[1,2] · M. E. Williams[2] · K.-W. Moon[2] · G. B. McFadden[3] ·
P. N. Patrone[3] · J. H. Perepezko[4]

Abstract Diffusion couple experiments between Ni and Re at 1200 and 1350 °C were performed. These experiments established the limits of the two-phase FCC + HCP region. No intermediate phase was observed at these temperatures. Composition-dependent interdiffusion coefficients and associated uncertainties were estimated by three methods. The first employed fitting of the penetration curves in conjunction with the Sauer-Freise (SF) method. The second method employed a numerical solution of the Boltzmann-Matano ordinary differential equation for composition-dependent interdiffusion coefficient functions whose parameters were optimized by a least squares fitting to the data. Discrepancies between the results of these methods indicate typical uncertainties in experimental determination of diffusion coefficients. To further assess such discrepancies, a third method was employed to perform an uncertainty quantification of the diffusion coefficients via a statistical analysis based on the SF method.

Keywords alloy · binary diffusion · composition profiles · diffusion couples · experimental study

✉ W. J. Boettinger
   william.boettinger@nist.gov

1 Theiss Research, La Jolla, CA 92037, USA

2 Materials Science and Engineering Division, NIST,
   Gaithersburg, MD 20899, USA

3 Applied and Computational Mathematics Division, NIST,
   Gaithersburg, MD 20899, USA

4 Department of Materials Science and Engineering, University
   of Wisconsin, Madison, WI 53706, USA

1 Introduction

The Ni-Re alloys system is the subject of research because of the importance of Re as an alloying addition to Ni-based superalloys. The phase diagram of the Ni-Re system consists of a peritectic reaction between liquid and the Re-rich hexagonal-close-packed (HCP) solid phase to form the Ni-rich face-centered-cubic (FCC) solid phase.[1,2] Recent research[3] has suggested the existence of an additional phase, Ni_4Re, isomorphous with Ni_4Mo having the $D1_a$ structure that is an ordered variant of the FCC structure. Although this phase is thought to be stable only at low temperatures, the present work was conducted in part to determine whether this phase might be present at high temperatures where it might affect the solidification microstructure development. The diffusion couple experiments were also analyzed to reexamine the composition dependence of the interdiffusion coefficients in the FCC and HCP phases and to establish the uncertainty of these measurements.

Diffusion in the Ni-Re system has been studied by several authors. Neubauer et al.[4] performed diffusion experiments with pure Ni and pure Re end members at 990, 1050 and 1110 °C. They employed the Boltzmann-Matano method to obtain the value of the interdiffusion coefficient, $\tilde{D}$, at different compositions in the Ni-rich (FCC) and Re-rich (HCP) phases and determined the solubility limits of the FCC and HCP phases as approximately 10% Re and 75% Re, respectively. (All alloy compositions will be given in atomic percentages unless otherwise noted.) They reported no intermediate phase in this system at these temperatures. Karunaraste et al.[5] extracted concentration-dependent interdiffusion coefficients for the FCC phase using diffusion couples between pure Ni and Ni-10% Re

(mass) at temperatures between 900 and 1200 °C. They found very little concentration dependence (a factor of two at most). The data obtained by Ref 6 was used for handbook values for impurity diffusion of Re in Ni. At the temperatures of the present study, 1200 and 1350 °C, these values are 7.43×10^{-16} and 5.09×10^{-15} m^2/s, respectively. Zeng et al.[7] extracted interdiffusion coefficients in the FCC phase from diffusion couples between Ni-1% Re (mass) and Ni-4.8% Re (mass) at 1100, 1150, 1200 and 1250 °C. Hobbs et al.[8] report average values in the FCC phase of 6.12×10^{-18} and 9.31×10^{-17} m^2/s at 1000 and 1100 °C, respectively. Epishina et al.[9] performed diffusion couple measurements for Ni-Re in the FCC region up to 9% Re (mass) at temperatures between 1050 and 1350 °C. They observed no significant concentration dependence. This prior research is summarized in Table 1 and plotted in Fig. 1.

The present paper analyzes the results of diffusion couple experiments in order to determine (1) the composition-dependent interdiffusion coefficients, (2) the composition limits of the two phase FCC + HCP region in the phase diagram, and (3) associated uncertainties in these quantities. To this end, we invoke three separate methods for analyzing the experimental data, each providing their own independent assessment of their corresponding uncertainties.

2 Experiments

Diffusion couples were prepared from 5 mm cubes of Ni and Re with 99.99% purity. The pure Ni end member was cut from a swaged rod. The pure Re end member was cut from an arc cast rod. Couples consisted of a Ni/Re/Ni stack where the touching faces were polished to a metallographic grade finish. A molybdenum alloy clamp was used. Two samples were sealed separately in evacuated quartz ampoules and annealed at 1350 °C for 5 h and at 1200 °C for 160 h, respectively. Sectioning and polishing parallel to the diffusion direction revealed no microstructure or porosity. Microprobe analysis was performed using elemental standards with 1 nA current at 15 kV with a counting time of 400 s with a 1 μm spacing, a spacing that
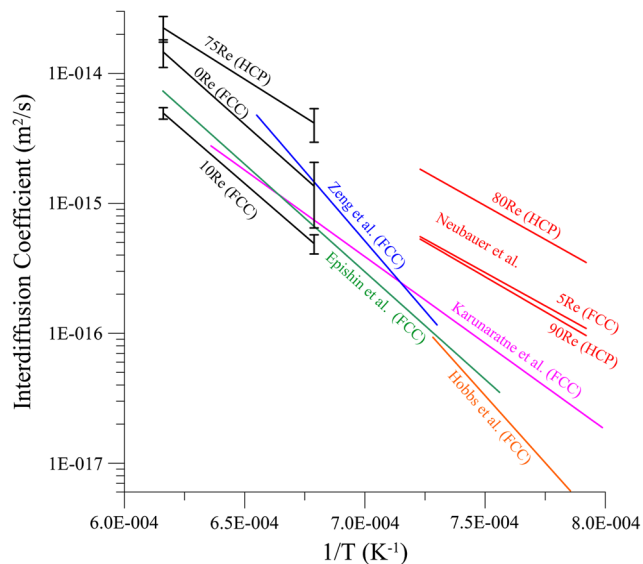

Fig. 1 Arrhenius plots (colored lines) of various data sets from the literature shown in the temperature range where measured. Black lines with error bars show results from the present work for selected compositions

corresponds to the approximate x-ray excitation volume size in the sample. The Ni K and Re L lines were employed. One sigma error of the measured Re content given by the microprobe software is approximately 0.03% Re in the Ni-rich FCC phase and 0.3% Re in the Re-rich HCP phase. Two line scans from each diffusion couple were employed and are referred to as 1200 A, 1200 B, 1350 A and 1350 B.

Chemical etching of the diffusion couples after microprobe measurements revealed the grain structure. The grain size of the FCC phase was approximately 100-500 μm. The grain size of the HCP phase was on the order of 10-40 μm. Because the diffusion distance in the HCP phase was on the order of 50 μm, the contribution to diffusion in the HCP by grain boundaries cannot be excluded.

The molar volume $V_m(x_{Re})$ as a function of atomic (mole) fraction Re, x_{Re}, was assumed to obey a common volume-based Vegard's Law (constant partial molar volumes) for both the FCC and HCP phases. Using the molar volume values for pure Ni and Re from Ref 10, the molar volume in (m^3/mole) for the alloy is taken as

References	D_0 (m^2/s)	Q (kJ/mole)	Comment
Table 1 Summary of literature on measurements of interdiffusion coefficients in Ni-Re, $\tilde{D} = D_0 \exp[-Q/RT]$			
4	1.4E−8	196	FCC 5% Re, 900 to 1150 °C
4	6.0E−8	199	HCP 80% Re, 900 to 1150 °C
4	3.2E−8	206	HCP 90% Re, 900 to 1150 °C
5	8.2E−7	255	FCC 0-10% Re (mass), 900 to 1300 °C
7	5.96E−1	412	FCC 1-4.8% Re (mass), 1100 to 1250 °C
9	1.16E−4	317	FCC 0-9% Re (mass), 1050 to 1350 °C

$$V_m = 6.586 \times 10^{-6}(1 - x_{Re}) + 8.849 \times 10^{-6}x_{Re}. \quad \text{(Eq 1)}$$

3 Diffusion Equation

For constant partial molar volumes, the diffusion equation in a reference frame moving with the local center of volume is

$$\frac{\partial c_{Re}}{\partial t} = \frac{\partial}{\partial z}\left(\tilde{D}\frac{\partial c_{Re}}{\partial z}\right), \quad \text{(Eq 2)}$$

where $c_{Re}(z, t)$ is the concentration (moles/m³), z is the spatial coordinate (m), and t is the time (s) of the diffusion anneal. The concentration is obtained from the measured atomic fraction profile $x_{Re}(z, t)$ via

$$c_{Re}(z, t) = x_{Re}(z, t)/V_m(x_{Re}(z, t)).$$

For the conditions of infinite diffusion couples, the Boltzmann-Matano transformation

$$\xi = \frac{z - z_0}{t^{1/2}}, \quad c_{Re}(z, t) = C(\xi), \quad \text{(Eq 3)}$$

reduces Eq 2 to the ordinary differential equation

$$-\frac{\xi}{2}\frac{dC}{d\xi} = \frac{d}{d\xi}\left(\tilde{D}\frac{dC}{d\xi}\right). \quad \text{(Eq 4)}$$

The appropriate boundary conditions for Eq 4 are that $C(\xi) \to C^{\pm}$ as $\xi \to \pm\infty$, where $C^{\pm} = x_{Re}^{\pm}/V_m(x_{Re}^{\pm})$ are the far-field solute concentrations. There is also a conservation jump condition relating the jumps in flux and concentration at the moving FCC-HCP phase boundary position z_{phase}. The Matano interface position is obtained by finding the value z_0 that satisfies the equation

$$\int_{-\infty}^{z_0}\left[c_{Re}(z) - c_{Re}^-\right]dz = \int_{z_0}^{\infty}\left[c_{Re}^+ - c_{Re}(z)\right]dz. \quad \text{(Eq 5)}$$

For simplicity we henceforth suppress the explicit time dependence in $c_{Re}(z, t)$ and $x_{Re}(z, t)$; the time will always correspond to the time of the diffusion anneal.

Finally, the interdiffusion coefficient can be obtained by the Sauer-Freise equation in either of its forms:

$$\tilde{D}(z) = \frac{1}{(c_{Re}^+ - c_{Re}^-)}\frac{1}{2t(dc_{Re}/dz)}\left[(c_{Re}^+ - c_{Re}(z))\int_{-\infty}^{z}(c_{Re}(z') - c_{Re}^-)dz' \right.$$
$$\left. + (c_{Re}(z) - c_{Re}^-)\int_{z}^{\infty}(c_{Re}^+ - c_{Re}(z'))dz'\right],$$
$$\text{(Eq 6)}$$

$$\tilde{D}(z) = \frac{V_m(x_{Re}(z))}{x_{Re}^+ - x_{Re}^-}\frac{1}{2t(dx_{Re}/dz)}\left[(x_{Re}^+ - x_{Re}(z))\int_{-\infty}^{z}\frac{(x_{Re}(z') - x_{Re}^-)}{V_m(x_{Re}(z'))}dz' \right.$$
$$\left. + (x_{Re}(z) - x_{Re}^-)\int_{z}^{\infty}\frac{(x_{Re}^+ - x_{Re}(z'))}{V_m(x_{Re}(z'))}dz'\right].$$
$$\text{(Eq 7)}$$

Technically the interdiffusion coefficients from Eq 6 and 7 are with respect to the center of moles and center of mass respectively. But for a binary alloy with constant partial molar volumes as assumed in the present case, these interdiffusion coefficients are identical.[11–13]

4 Results and Analysis

4.1 Experimental Data

Figure 2 and 3 show the measured penetration data points for 1200 and 1350 °C respectively plotted as $x_{Re}(\xi)$ along with the fits described below. The jump in composition at the interface between the FCC and HCP phases is clearly shown and the Matano positions for all diffusion couples, $\xi = 0$, lie within the HCP phase indicating that the FCC phase is dissolving and the HCP phase is growing. There is no evidence of any intermediate phase at the temperatures studied.

The diffusion profiles in the HCP phase have a sharp transition to pure Re. The curves fail to become shaped like an error function for large ξ on the scale of the measurement spacing. A similar shape was observed on the Ni-rich side of Au-Ni diffusion couples.[14,15] Indeed, backscatter images of the diffusion couple show an apparent sharp change in contrast at this location that can be confused with a phase interface. Significant data scatter is seen on the HCP side of the diffusion couple. This is presumably due to the small grain size of the Re end member.

4.2 Assessment of $\tilde{D}$ Using the Sauer-Freise Approach

Three different analysis methods were used in the present research in order to gain insight into the uncertainty. In the first approach (the "Sauer-Freise method") the atomic fraction Re data $x_{Re}(z)$ was fit using a commercial software package separately for the FCC and HCP phases. For the FCC phase a function was used that guaranteed a zero slope at minus infinity; viz.,

$$x_{Re}(z) = a\exp(z/b)(1 + cz + dz^2), \quad \text{(Eq 8)}$$

where the lower case letters are fitting parameters. For the HCP side the following function captured the general shape of the penetration curve while still having a relatively smooth derivative,

$$x_{Re}(z) = a + bz + cz^2 + dz^3 + e\exp(z). \quad \text{(Eq 9)}$$

The exponential term in Eq 9 was found necessary to capture the diffusion profile near the Re end member. The fits are shown as the red lines in Fig. 2 and 3. The residuals
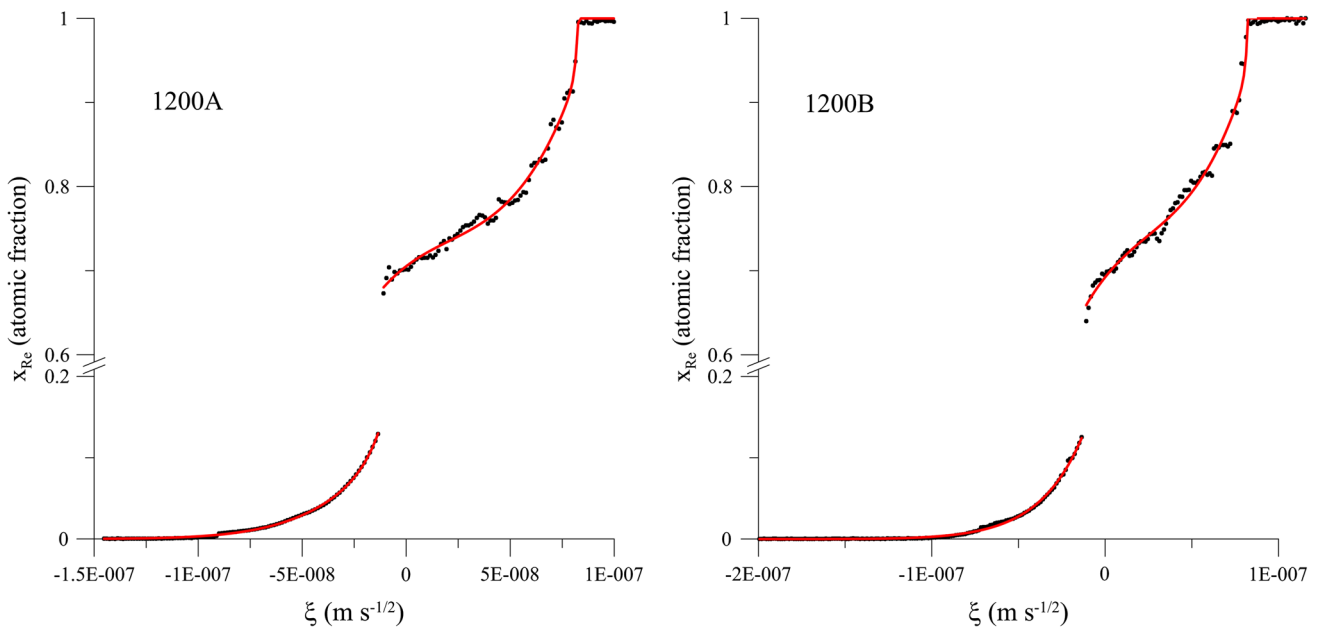
Fig. 2 Measured composition vs. scaled distance for diffusion at 1200 °C for 160 h (pts.) and fit (red curve) used for the Sauer-Freise integration
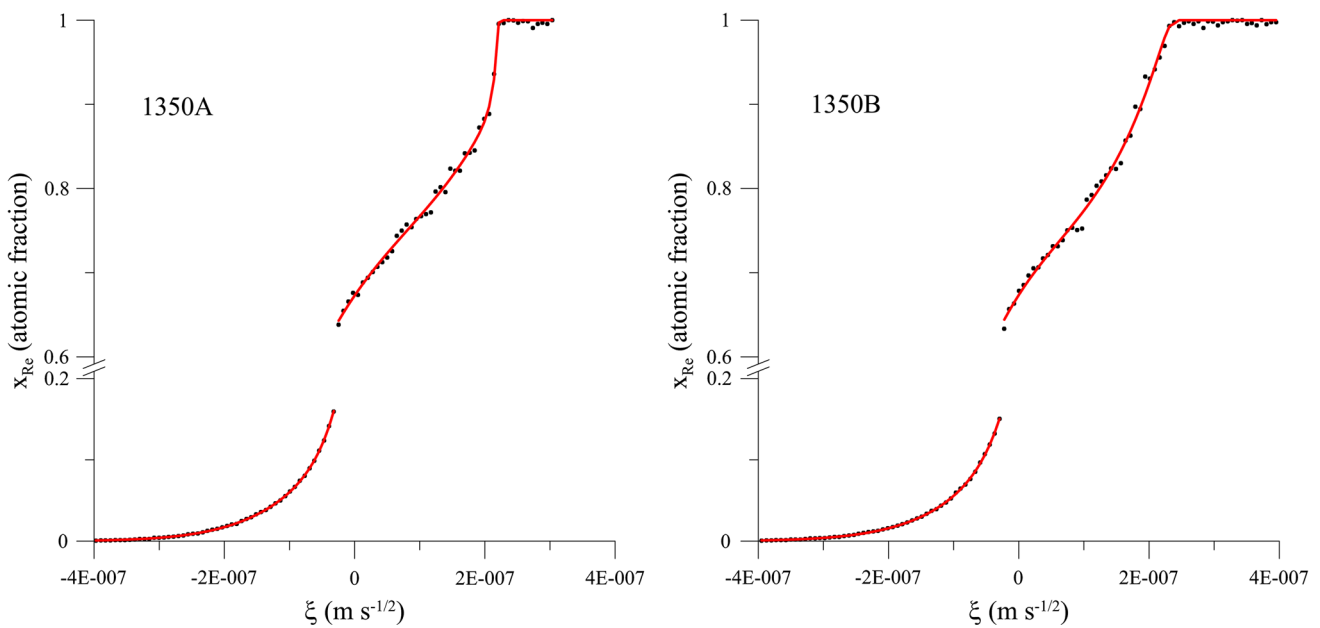

Fig. 3 Measured composition vs. scaled distance data for diffusion at 1350 °C for 5 h(pts.) and fit (red curve) used for the Sauer-Freise integration

(observed minus fit) are shown in Fig. 4 and 5 along with the residuals for the other methods described below (the "ODE method" and the "UQ method").

From fits to the diffusion profiles, the compositions on either side of the interphase interface can be established. Under the assumption of local equilibrium, usually valid for diffusion couples at late times, these values establish the solubility limits of Re in FCC Ni and Ni in HCP Re.

The results are summarized in Tables 2 and 3. Table 2 also gives the same information obtained from the other two approaches. Upper and lower bound estimates are also given. These bounds were determined by a procedure that examined the uncertainties of profile fits and the interface position, which cannot be resolved experimentally to better than the 1 μm spacing of the microprobe measurements. The ranges are not symmetric about the determined value.
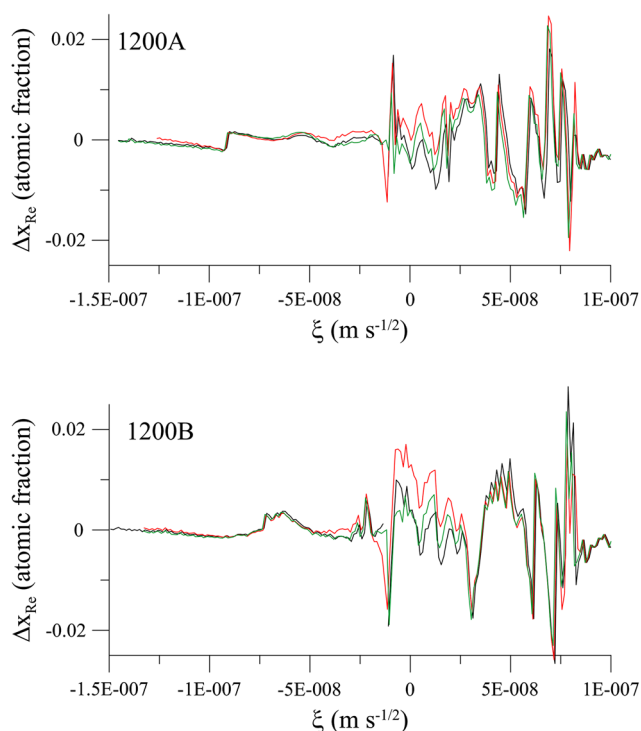
Fig. 4 Deviation of measured data from fits for 1200 °C diffusion profiles. S-F method (black), ODE method (red) and UQ method (green)
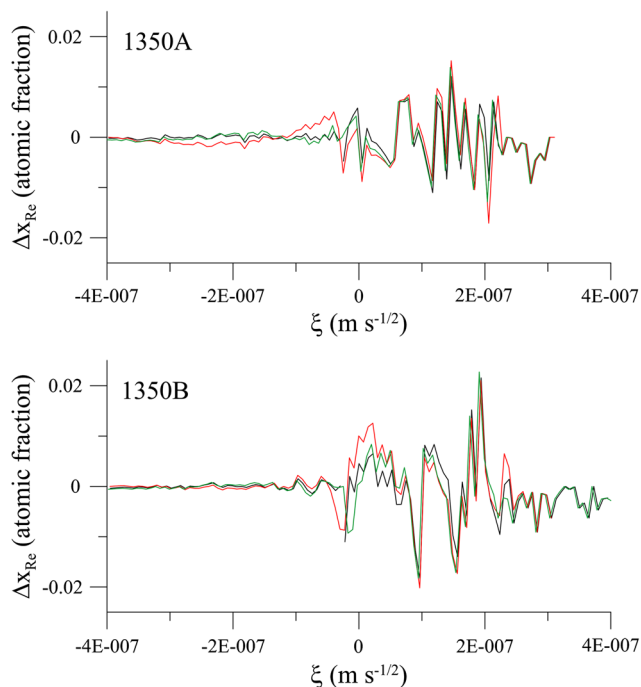

Fig. 5 Deviation of measured data from fits for 1350 °C diffusion profiles. S-F method (black), ODE method (red) and UQ method (green)

In Table 3 the mean and standard deviation obtained from the six numbers from the three methods and A and B profiles are given along with the phase boundary values determined by Ref 1.

To obtain interdiffusion coefficients with the Sauer-Freise approach, Eq 7 was employed. The integration was performed using a piecewise function formed from the two fitting functions, Eq 8-9, for each data set in Mathematica.[1] The interdiffusion coefficient values as a function of composition are shown as discrete points from each data set at 1200 °C and at 1350 °C in Fig. 6 for the FCC and HCP phases. Additional lines are shown that are obtained from the other methods as described below. As usual with the Sauer-Freise method, the values near the end members (0 and 100% Re) are not reliable. The diffusion coefficients for the FCC at each temperature are in good agreement: the composition-dependent value of $\tilde{D}$ is observed to decrease with increasing Re content by a factor of three over the range of solubility. For the HCP phase the agreement between the two data sets at each temperature is not as good as for the FCC phase, undoubtedly due to the larger noise in the measured HCP penetration curve data. However, the HCP data at both temperatures show a maximum at approximately 75% Re (mole fraction). The dramatic drop of the values of $\tilde{D}$ by a factor of ten or more as the composition approaches pure Re is evident, a fact consistent with the very sharp rises toward 100% Re in the composition versus distance curves.

4.3 Assessment of $\tilde{D}$ Using an Ordinary Differential Equation (ODE) Solver

A second approach (the "ODE method") can be used to determine the diffusion coefficients $\tilde{D}(x_{Re})$ for the FCC and HCP phases from the measured solute profiles $x_{Re}(z)$. This method solves the Boltmann-Matano Eq 4 iteratively, updating guesses for $\tilde{D}(x_{Re})$ until satisfactory agreement is attained between the computed and measured profiles for $x_{Re}(z)$. Such a method has been applied to single phase ternary diffusion couples by Ref 16. In the present two phase diffusion couple, the functional form of the unknown diffusion coefficient $\tilde{D}(x_{Re})$ is assumed to be given in terms of a small set of fitting parameters,

$$\tilde{D}(x_{Re}) = \begin{cases} \exp\left[A_0 + A_1 x_{Re} + A_2(x_{Re})^2\right], & \text{in the FCC phase } (z < z_{phase}) \\ \exp\left[B_0 + B_1 x_{Re} + B_2(x_{Re})^2\right], & \text{in the HCP phase } (z > z_{phase}). \end{cases}$$

(Eq 10)

Given the far-field concentrations and the concentrations at the phase boundary, and guesses for the parameters, A_j and B_j, and the Matano position, z_0, the ordinary differential Eq 4 is solved numerically to obtain a computed solution. The difference between the computed solute

---

[1] ◆ Mention of trade names is for completeness only and does not constitute an endorsement by the National Institute of Standards & Technology.

Table 2 Summary of solubility limits (%) established from the Sauer-Freise method, the ODE method and the UQ method: value (lower bound, upper bound)

	FCC limit SF	FCC limit ODE	FCC limit UQ	HCP limit SF	HCP limit ODE	HCP limit UQ
1200 A	13.0 (12.9, 14.2)	13.7 (13.0, 15.1)	14.2 (12.2, 16.4)	68.0 (66.9, 68.8)	68.3 (68.2, 68.5)	68.8 (67.1, 69.8)
1200 B	12.4 (12.3, 13.3)	13.5 (13.1, 15.1)	13.5 (12.3, 15.1)	65.4 (64.4, 66.8)	65.0 (64.8, 65.6)	66.5 (63.9, 68.2)
1350 A	16.0 (15.9, 18.5)	16.6 (15.9, 18.7)	17.5 (15.8, 19.7)	64.3 (62.3, 65.1)	63.7 (63.3, 64.5)	63.5 (61.3, 65.2)
1350 B	15.0 (14.9, 17.2)	16.3 (15.9, 18.7)	16.2 (14.9, 18.6)	64.4 (62.0, 65.5)	65.0 (64.8, 65.6)	65.0 (63.1, 66.5)

Table 3 Mean and standard deviations of solubility limits determined by the three methods for the A and B data sets

T, °C	FCC limit % Re	HCP limit % Re	FCC limit[1]	HCP limit[1]
1200	13.4 ± 0.6	67.0 ± 1.6	14.6	71
1350	16.3 ± 0.8	64.3 ± 0.6	16.8*	68*

* Interpolated from data at 1200 and 1500 °C

profile and the experimental data is then used to generate an improved guess for the unknown parameters, and the process is repeated until convergence is obtained. Details about the numerical procedure are provided in Appendix 1. With this approach it is not necessary to fit the measured data with empirical functions, as is required to apply the Sauer-Freise technique. If the numerical solution to Eq 4 is determined over a large enough finite interval of ξ, the computed solution asymptotes to the far-field values with negligible solute gradients there, so the self-similarity assumptions of the Boltzmann-Matano equation are satisfied.

In practice we find that a good fit to the data can be obtained by using a linear expression for $\ln \tilde{D}(x_{Re})$ in the FCC phase in Eq 4 with $A_2 = 0$, whereas a quadratic equation is more accurate in the HCP phase. The optimized parameters for the interdiffusion coefficients as defined in Eq 10 for the four data sets are given in Table 4 and the values of $\tilde{D}(x_{Re})$ are plotted in Fig. 6. An example of the quality of the fit using the ODE method is shown in Fig. 7 along with a magnified view of the region near the Re end of the couple. The decrease in the diffusivity as the composition approaches pure Re produces a distinct shoulder in the computed solute profile in the HCP phase, which the solution to the Boltzmann-Matano equation is able to reproduce quantitatively. The residuals for the ODE method are shown in Fig. 4 and 5 and are remarkably similarity to those obtained from the Sauer-Freise method.

Taking means of the parameters for the two data sets at each temperature from Table 4, one can determine the composition dependence of the prefactor, D_0, in (m²/s) and the activation energy, Q, in (kJ/mole) in the expression $\tilde{D} = D_0 \exp[-Q/RT]$. For the FCC phase we obtain

$$\begin{aligned} \ln D_0 &= -8.52 - 17.2 x_{Re}, \\ Q &= 314.9 - 85.9 x_{Re}, \end{aligned} \tag{Eq 11}$$

and for the HCP phase we obtain

$$\begin{aligned} \ln D_0 &= -57.3 + 81.3 x_{Re} - 33.0 x_{Re}^2, \\ Q &= 49.6 + 3.5 x_{Re} + 304 x_{Re}^2. \end{aligned} \tag{Eq 12}$$

For pure Ni this gives $\ln D_0 = -8.52$ and $Q = 314.9$ in the units stated above. For pure Re this gives $\ln D_0 = -9.0$ and $Q = 357.1$.

4.4 Assessment of $\tilde{D}$ and Uncertainty Quantification (UQ) Using a Statistical Method

The third approach, a statistical uncertainty quantification method (the "UQ method"), tries to reconcile differences between the previous methods by independently estimating uncertainties in $\tilde{D}(x_{Re})$. This third approach, which is based on the Sauer-Freise method, is comprised of two main steps. First, a smooth function is fit to the penetration profile and the associated residuals (i.e. measured minus fit) are used to construct a noise model. This model is formulated so as to partially compensate for small systematic deviations of the fit relative to the data, thereby making the choice of the fitting function less critical. Second, the noise model is numerically sampled to rapidly create multiple (e.g., 1000) synthetic penetration profiles. Refitting each synthetic penetration profile and analyzing each with the SF formula results in a distribution of diffusion coefficients that should be consistent with the noise in the underlying data. From this distribution, it is straightforward to extract mean diffusion coefficients and uncertainties as needed.

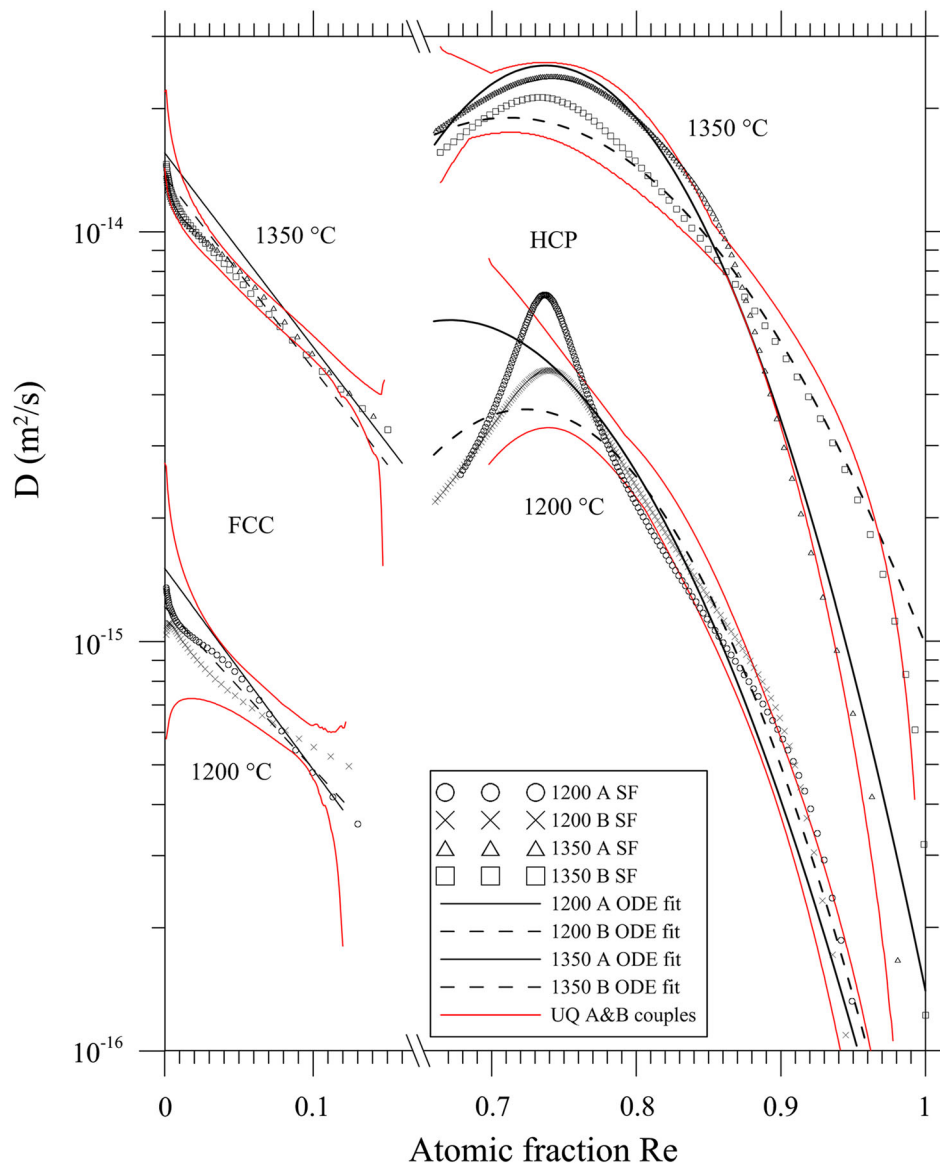We begin by examining fits to and residuals of the data using the function

Fig. 6 Composition dependence of the interdiffusion coefficient obtained for the Ni-rich FCC phase and the Re-rich HCP phase by two methods at 1350 and 1200 °C: S-F method (points), ODE method (black lines). Upper and lower uncertainty bounds ($\pm 3\sigma$) established by the UQ method (red lines)

$$x_{\mathrm{Re}}(z) = x_{\mathrm{Re}}^{-} + f(z)\{1 - \mathrm{erf}\,[a_5(z - z_{\mathrm{phase}})]\}$$
$$+ h(z)\{1 + \mathrm{erf}\,[a_5(z - z_{\mathrm{phase}})]\}\Theta(z_{\mathrm{corner}} - z)$$
$$+ x_{\mathrm{Re}}^{+}\Theta(z - z_{\mathrm{corner}}),$$

$$\text{(Eq 13)}$$

where

$$f(z) = (a_1/2)\{1 + \mathrm{erf}\,[a_2\mathrm{sgn}(z - a_3)|z - a_3|^{a_4}]\},$$
$$h(z) = (a_7/2)\left\{1 + a_8\mathrm{erf}^{-1}[a_9(z - a_{10})]\right\},$$

$$\text{(Eq 14)}$$

and $\mathrm{sgn}(x) = \pm 1$ is the sign of x, $\Theta(x)$ is the Heaviside step function, and the erf^{-1} function is the inverse error function restricted to the domain over which it is strictly real. The position z_{corner} is the location where the extremely

sharp transition of the penetration curve to pure Re occurs. As such it satisfies $h(z_{\mathrm{corner}}) = x_{\mathrm{Re}}^{+}$, where it is further assumed that $(1/2)\left\{1 + \mathrm{erf}\,[a_5(z - z_{\mathrm{phase}})]\right\} \approx 1$ at the corner, or equivalently, that a_5 is large relative to the horizontal spacing of the data points. The profiles in the FCC and HCP phases have different behaviors characterized by $f(z)$ and $h(z)$, respectively. The terms $\left\{1 \pm \mathrm{erf}\,[a_5(z - z_{\mathrm{phase}})]\right\}$ act as switching functions that allow the penetration profile to transition between these two behaviors. At the sharp phase-transition interface, we expect the concentration profile to change over a characteristic length-scale equal to the spacing of the measurement. This sets a lower limit on plausible values of $1/a_5$. Moreover, by symmetry of the error function, we also

Table 4 Optimized parameters for $\tilde{D}(x_{Re})$ in Eq 10 obtained from the four data sets

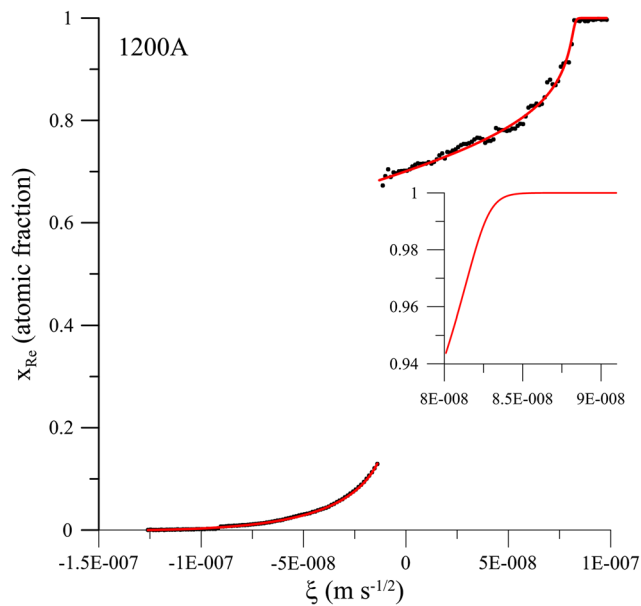| Set	A_0	A_1	A_2	B_0	B_1	B_2
1 (1350 A)	−31.792434	−10.906097	0	−72.292549	111.18898	−75.399494
2 (1350 B)	−31.926384	−10.78129	0	−49.728444	50.930777	−35.760985
3 (1200 A)	−34.128757	−11.300799	0	−55.980823	69.271011	−51.600557
4 (1200 B)	−34.343263	−9.0894963	0	−66.789142	92.796541	−64.15788

Fig. 7 Example of fit using ODE method for 1200 A data. Inset shows ODE solution near $x_{Re} = 1$

identify a_6 as the interface position, z_{phase}. The residuals of the fits using Eq 13 and 14 are given in Fig. 4 and 5. They are very similar to those obtained from the other methods.

To construct the noise model, we treat the residuals (cf. Fig. 4 and 5) as a random sample of the noise in our data. By eye, it is obvious that these residuals have structure as a function of distance. Given this observation, there are many reasonable procedures for constructing a noise model. Here we invoke a Gaussian-process analysis[17] that views the residuals as evaluations of a random function with an undetermined smoothness and spatial correlation structure characterized in terms of a set of free parameters ϕ (see Appendix 2). Importantly, individual points on this function are Gaussian random variables, while collections of points are multivariate Gaussian random variables with a covariance determined partially by the data. While details of this analysis are provided in Appendix 2, we note here that this procedure yields j synthetic concentration profiles of the form

$$x^j_{Re,synth}(z_i) = x_{Re}(z_i) + \eta^j(z_i; \varphi), \qquad (Eq\ 15)$$

where $x_{Re}(z_i)$ is the fit, Eq 13, evaluated at the discrete points, z_i, and η^j is the jth realization of the postulated noise model with parameters ϕ determined to match the spatial correlation structure of the experimental residuals (see Appendix 2). Therefore, the synthetic noise realizations have (random) features that are qualitatively similar to those of the residuals in Fig. 4 and 5.

Given the specification of the noise model (via the parameters ϕ), we then use random number generators to create on the order of 1000 realizations of $x^j_{Re,syn}(z_i)$, each of which is subsequently analyzed using the Sauer-Freise formalism. Figure 8 shows an example of five fits to synthetic $x_{Re}(\xi)$ profiles generated for the 1200 A data. Notably, the profiles show a much larger spread on the Re-rich side of the diffusion couple, consistent with the larger scatter in the data there. The insets in Fig. 8 show examples of a synthetic penetration curve. Its noise is similar to the raw data.

Given the 1000 determinations of $\tilde{D}(x_{Re})$, we then compute an average diffusion coefficient and standard deviation at each composition over the synthetic sets. Figure 6 includes the combined $\pm\,3$ sigma uncertainties of the A and B data sets for the composition-dependent interdiffusion coefficient as red lines. The choice of three times the standard deviation is somewhat arbitrary and was chosen because the residuals are not Gaussian. Chebyshev's rule states that at least 89% of data lie within three standard deviations in such cases.

For the 1200 °C FCC case (Fig. 6) the uncertainty in the determination of $\tilde{D}$ expands in the positive and negative directions near pure Ni and near the limit of solubility of the FCC phase. A similar expansion of the uncertainty ranges near the HCP solubility limit are noted. The expansion of the uncertainty bounds near pure Ni reflects the usual difficulty of the SF method and/or the end corrections described in Eq 17 below. Near the phase boundary the increase in uncertainty is likely due to uncertainty in fitting end of range data. The reason that the uncertainty range for the 1350 °C FCC diverges in only the positive directions near pure Ni is a result of the smaller values determined for the exponent, a_4, in Eq 14 generated by fitting of the synthetic data generated by the noise model.
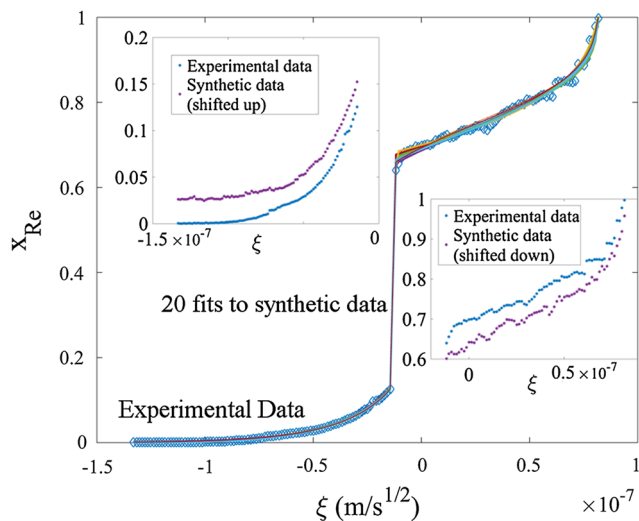
758

J. Phase Equilib. Diffus. (2017) 38:750–763

Fig. 8 Plot of measured profile for Set 1200 A (diamonds) and fits to five synthetic data sets(lines). The insets show original data for the FCC and HCP regions and an example of synthetic data for each

5 Discussion

The interdiffusion coefficients and the associated uncertainties have been determined for the FCC and HCP phases in the Ni-Re system at 1200 and 1350 °C as summarized in Fig. 6. Three methods were employed: a traditional Sauer-Freise method, a method that solved the diffusion equation for composition-dependent interdiffusion coefficients and a Sauer-Freise method using different fitting functions that were applied to synthetic data generated from a statistical model of the noise in the experimental data. The agreement of the $\tilde{D}$ values obtained by the three methods for the FCC phase are within a factor of 1.3 at intermediate compositions in the FCC solubility range. Agreement of a factor of two occurs near pure Ni and near the solubility limit. For the HCP phase the three methods give results that differ by a factor of two except near the HCP solubility limit where the deviation is a factor of seven.

For the FCC phase over its solubility range, $\tilde{D}$ decreases by a factor of three with increasing Re content at 1200 °C and by a factor of 4.5 at 1350 °C. The limiting value of $\tilde{D}$ as $x_{Re} \rightarrow 0$ corresponds to the Re impurity diffusion coefficient in FCC Ni. The values obtained by the ODE method for 1200 and 1350 °C respectively are 1.35×10^{-15} and 1.46×10^{-14} m^2/s respectively. As can be seen in Fig. 1, the values from the present work are larger than those of Ref 5 which were selected by Ref 6 as reference values for impurity diffusion of Re in Ni. The activation energy obtained for the diffusion in the FCC phase in the present work is given by Eq 11. Its value ranges from 314.9 kJ/mole as $x_{Re} \rightarrow 0$ to 306.3 kJ/mole at

$x_{Re} = 0.1$. This agrees most closely with the value reported by Ref 9 of 317 kJ/mole (Table 1).

For the HCP phase a maximum value of $\tilde{D}$ is observed near 75% Re at each temperature. The interfusion coefficient decreases by a factor of 10 or more as pure Re is approached at each temperature.

In addition to the results of Fig. 6, Table 5 gives the mean and standard deviation of the 6 determinations of $\tilde{D}$ at selected compositions at 1200 and 1350 °C. In general, but not always, the bounds provided by the UQ method (red lines in Fig. 6) are about plus and minus two times the standard deviations given in Table 5.

As a byproduct of the fitting of the diffusion penetration curves near the FCC-HCP phase interface in the diffusion couples, the compositions at the moving FCC/HCP interface have been determined by the three methods. Under the assumption of local equilibrium usually valid for diffusion couple experiments at long times, these numbers give the boundaries of the FCC + HCP two phase region in the Ni-Re system. At 1200 °C the mean values for the FCC and HCP phases from Tables 2 and 3 are 13.4% Re and 67.0% Re, respectively. At 1350 °C the mean values for the FCC and HCP phases are 16.3% Re and 64.3% Re, respectively. The uncertainty of these values can be assessed by examination of the minimum and maximum values for these parameters that are given in Tables 2 and 3. No intermediate phase was observed in the diffusion couples. The solubility limits for the FCC and HCP phases obtained in this work can be compared to those measured by Ref 1 at 1200 °C of 14.6% Re and 71% Re. Their FCC value is within the uncertainty estimate for the FCC but their value for HCP is outside the uncertainty limits.

Formal uncertainty limits for these quantities were established by generating synthetic penetration curves based on the statistics of the deviation of the experimental data from fits. Applying the Sauer-Freise method to each of these synthetic penetration curves gave a corresponding $\tilde{D}(x_{Re})$ curve. These 1000 curves were examined to established upper and lower bounds on the diffusion coefficients. These bounds approximated the variations observed using the initial Sauer-Freise method and the ODE method; see Fig. 6. Regarding these uncertainty estimates, it is worth noting that the analysis operates in a relatively data poor regime insofar as there are only two penetration profiles each for samples annealed at 1200 and 1350 °C. As such, traditional notions of uncertainty, e.g. characterized in terms of standard errors, may be unreliable, since the available data is insufficient to inform statistical information about an underlying probability density. Rather, the analysis should be viewed as an attempt to quantify the extent to which one can identify a ''unique'' interdiffusion coefficient given noise in the data

Table 5 $\tilde{D}$ versus x_{Re}, mean and standard deviation in m^2/s

FCC at 1200 °C			HCP at 1200 °C			FCC at 1350 °C			HCP at 1350 °C		
x_{Re}	Mean	Std	x_{Re}	Mean	Std	x_{Re}	Mean	Std	x_{Re}	Mean	Std
0.005	1.24E−15	1.29E−16	0.68	3.65E−15	1.64E−15	0.005	1.33E−14	1.14E−15	0.66	1.64E−14	9.65E−16
0.010	1.15E−15	1.15E−16	0.69	3.86E−15	1.24E−15	0.010	1.22E−14	1.05E−15	0.67	1.83E−14	1.85E−15
0.015	1.08E−15	1.06E−16	0.70	4.44E−15	1.29E−15	0.015	1.14E−14	1.01E−15	0.68	1.93E−14	1.42E−15
0.020	1.03E−15	9.85E−17	0.71	4.57E−15	1.01E−15	0.020	1.07E−14	9.54E−16	0.69	2.02E−14	1.31E−15
0.025	9.78E−16	9.01E−17	0.72	4.71E−15	8.73E−16	0.025	1.02E−14	8.84E−16	0.7	2.09E−14	1.60E−15
0.030	9.35E−16	8.18E−17	0.73	4.85E−15	1.08E−15	0.030	9.68E−15	8.12E−16	0.71	2.16E−14	1.97E−15
0.035	8.95E−16	7.35E−17	0.74	4.77E−15	1.18E−15	0.035	9.22E−15	7.41E−16	0.72	2.20E−14	2.39E−15
0.040	8.58E−16	6.51E−17	0.75	4.40E−15	8.26E−16	0.040	8.79E−15	6.73E−16	0.73	2.21E−14	2.77E−15
0.045	8.22E−16	5.66E−17	0.76	3.96E−15	4.63E−16	0.045	8.38E−15	6.09E−16	0.74	2.20E−14	3.05E−15
0.050	7.88E−16	4.80E−17	0.77	3.54E−15	2.20E−16	0.050	8.00E−15	5.48E−16	0.75	2.17E−14	3.22E−15
0.055	7.56E−16	3.93E−17	0.78	3.16E−15	1.26E−16	0.055	7.63E−15	4.92E−16	0.76	2.11E−14	3.28E−15
0.060	7.24E−16	3.10E−17	0.79	2.80E−15	1.54E−16	0.060	7.28E−15	4.40E−16	0.77	2.02E−14	3.22E−15
0.065	6.94E−16	2.35E−17	0.80	2.48E−15	1.70E−16	0.065	6.95E−15	3.94E−16	0.78	1.91E−14	3.07E−15
0.070	6.65E−16	1.78E−17	0.81	2.18E−15	1.78E−16	0.070	6.63E−15	3.54E−16	0.79	1.80E−14	2.84E−15
0.075	6.37E−16	1.56E−17	0.82	1.91E−15	1.65E−16	0.075	6.33E−15	3.21E−16	0.8	1.67E−14	2.47E−15
0.080	6.11E−16	1.72E−17	0.83	1.67E−15	1.34E−16	0.080	6.04E−15	2.96E−16	0.81	1.53E−14	2.17E−15
0.085	5.85E−16	2.11E−17	0.84	1.45E−15	1.07E−16	0.085	5.76E−15	2.80E−16	0.82	1.40E−14	1.83E−15
0.090	5.61E−16	2.56E−17	0.85	1.24E−15	8.86E−17	0.090	5.50E−15	2.68E−16	0.83	1.26E−14	1.48E−15
0.095	5.37E−16	2.99E−17	0.86	1.06E−15	8.12E−17	0.095	5.25E−15	2.64E−16	0.84	1.13E−14	1.15E−15
0.100	5.14E−16	3.39E−17	0.87	8.99E−16	7.72E−17	0.100	5.02E−15	2.60E−16	0.85	9.98E−15	8.32E−16
0.105	4.92E−16	3.72E−17	0.88	7.59E−16	8.77E−17	0.105	4.79E−15	2.61E−16	0.86	8.74E−15	6.69E−16
0.110	4.70E−16	4.08E−17	0.89	6.25E−16	8.92E−17	0.110	4.58E−15	2.60E−16	0.87	7.47E−15	4.78E−16
0.115	4.48E−16	4.47E−17	0.90	5.10E−16	8.66E−17	0.115	4.37E−15	2.60E−16	0.88	6.34E−15	6.57E−16
0.120	4.25E−16	4.88E−17	0.91	4.09E−16	7.83E−17	0.120	4.17E−15	2.59E−16	0.89	5.30E−15	9.10E−16
			0.92	3.09E−16	5.18E−17	0.125	3.98E−15	2.55E−16	0.9	4.41E−15	1.09E−15
			0.93	2.28E−16	3.59E−17	0.130	3.80E−15	2.51E−16	0.91	3.65E−15	1.16E−15
			0.94	1.61E−16	1.90E−17	0.135	3.62E−15	2.45E−16	0.92	3.00E−15	1.17E−15
			0.95	1.15E−16	1.69E−17	0.140	3.45E−15	2.38E−16	0.93	2.45E−15	1.11E−15
			0.96	7.80E−17	1.35E−17	0.145	3.27E−15	2.38E−16	0.94	1.98E−15	1.02E−15
			0.97	5.35E−17	1.35E−17	0.150	3.12E−15	2.61E−16	0.95	1.57E−15	9.11E−16
			0.98	3.81E−17	1.58E−17	0.155	2.91E−15	2.79E−16	0.96	1.23E−15	7.85E−16
			0.99	2.40E−17	1.47E−17				0.97	9.25E−16	6.57E−16
									0.98	6.61E−16	5.42E−16
									0.99	3.90E−16	4.22E−16

and a model for the diffusion process. For extensions of this analysis that address analogs of standard error across many datasets (which we do not have), see papers on statistical inference of interlaboratory studies of key-comparison experiments.

In order to better understand the analytical underpinnings of uncertainty and the corresponding role of the sharp break of the penetration profiles near the pure Re end of the diffusion couples (where the measured gradient is not zero), a detailed examination of the end conditions was performed. The relation in Eq 5 for the Matano interface position z_0 and the Sauer-Freise expressions in Eq 6 and 7

apply to an idealized infinite diffusion couple for which the solute gradients vanish in the far-field. They both are obtained by taking appropriate limits of the relation derived by integrating Eq 4 over an interval $\xi_1 \le \xi \le \xi_2$ that lies in a single phase,

$$\int_{\xi_1}^{\xi_2} \xi \frac{dC(\xi)}{d\xi} d\xi = \tilde{D}(C(\xi_2)) \frac{dC(\xi_2)}{d\xi} - \tilde{D}(C(\xi_1)) \frac{dC(\xi_1)}{d\xi}$$

(Eq 16)

and using the relation between z and ξ at fixed t given in Eq 3. By using this expression, the generalization of Eq 5

760

J. Phase Equilib. Diffus. (2017) 38:750–763

for the Matano position for data collected over a finite length $z_L \leq z \leq z_R$ that spans both phases is then

$$
\int_{z_L}^{z_0} [c_{Re}(z) - c_{Re}(z_L)] \, dz - \int_{z_0}^{z_R} [c_{Re}(z_R) - c_{Re}(z)] \, dz
$$
$$
= 2t\tilde{D}(c_{Re}(z_R)) \frac{dc_{Re}(z_R)}{d\xi} - 2t\tilde{D}(c_{Re}(z_L)) \frac{dc_{Re}(z_L)}{d\xi},
$$
(Eq 17)

where the two terms on the right are end corrections that may be non-zero if the measured solute gradients at the ends of the range of data measurement are non-negligible. Similar end corrections to the Sauer-Freise Eq 6 and 7 can be obtained. When applying Eq 5, 6, or 7 to experimental data obtained over a finite distance range, it is important to check that the resulting end corrections are negligible. In our case, the experimental data for compositions that approach pure Re have steep and poorly resolved solute gradients. To avoid contributions from end corrections, the fits to the data should employ functions that extend beyond the experimental data set with extrapolations that have small gradients in the far field. The fits that are obtained using the ODE method can be explicitly checked for self-consistency by evaluating the Matano position expressions and Sauer-Freise expressions using the computed solution. By choosing a large enough fitting interval, we could obtain satisfactory agreement between all three methods.

The consideration of end corrections for a finite couple also enters into the question of uniqueness of diffusion coefficients that can be computed from experimental data. For example, the end-corrected Sauer-Freise expressions for data on a finite interval with non-negligible solute gradients shows that the resulting diffusion constants determined may not be unique, and depend on how the data near the end of the couple is treated. When Eq 5, 6, or 7 are applied for experimental data on a finite interval where the solute gradients are not small, this type of underlying non-uniqueness may be reflected in the relatively large magnitude of the uncertainties in the computed diffusion constants near the ends of the sample.

The ODE method in particular can be used to highlight the large uncertainties, or even non-uniqueness, in the diffusivities by its propensity to obtain good fits to the penetration curve data by using significantly different composition-dependent diffusivity functions. For example, by using starting estimates for the diffusion coefficients in the ODE method's iterative procedure that are obtained from various fits to the diffusivities obtained by the other two methods (for example, by assuming higher degree polynomial fits than assumed in Eq 10), diffusivities that lie at the extremes of the uncertainty intervals can easily be obtained.

Finally, we comment on the various optimizations performed in the present paper. The least square error of the fits $c_{Re}^{FIT}(z_j)$ to the experimental solute data $c_{Re}(z_j)$ at the positions $z_j, j = 1, 2, \ldots, N$, is denoted by

$$
E_{LS} = \left[\frac{1}{N} \sum_{j=1}^{N} |c_{Re}(z_j) - c_{Re}^{FIT}(z_j)|^2 \right]^{1/2}.
$$
(Eq 18)

The error E_{LS} is the quantity that is minimized in using the ODE method, and is also used to determine fits to the data in the other two methods. Whether this measure of error is the best one to use is perhaps an open question; for example, given the larger scatter in the experimental data in the HCP phase relative to the FCC phase, a version of least square error with unequal weights in each phase (or, for example, one that highlights the data near the phase boundary) might be preferable in some ways.

6 Conclusion

- The interdiffusion coefficients have been determined from diffusion couple experiments by three methods for the FCC and HCP phases in the Ni-Re system at 1200 °C and 1350 °C. Two of the methods employ the Sauer-Friese method but with different smoothing methods. The third (called the ODE method) determines an optimal $\tilde{D}(x_{Re})$ function by comparing the measured data to the solution to the diffusion equation. A linear $\tilde{D}(x_{Re})$ function was found adequate for the FCC phase, but a quadratic $\tilde{D}(x_{Re})$ function was necessary for the HCP phase. Higher order functions did not improve the fit, but cannot be excluded as possible results. The results are given from all three methods are shown in Fig. 6.

- Mean values for the diffusion coefficients obtained from the three methods are given in Table 5 along with the associated standard deviation.

- Composition dependent Arrhenius expressions deduced from the ODE results are given by Eq 11 and 12.

- The agreement of the three methods for the FCC phase are within a factor of 1.3 at intermediate compositions in the FCC solubility range. Agreement of a factor of two occurs near pure Ni and near the solubility limit. For the HCP phase the three methods give results that differ by a factor of two except near the HCP solubility limit where the deviation is a factor of seven and near pure Re where the deviation is more than a factor of 30.

- For the FCC phase over its solubility range, $\tilde{D}$ decreases by a factor of three with increasing Re content at 1200 °C and by a factor of 4.5 at 1350 °C. The limiting value of $\tilde{D}$ as $x_{Re} \to 0$ corresponds to the Re impurity diffusion coefficient in FCC Ni. The values

obtained by the ODE method for 1200 °C and 1350 °C, considered more reliable in this limit than the SF method, are 1.35×10^{-15} and 1.46×10^{-14} m^2/s respectively.

- For the HCP phase, a maximum value of $\tilde{D}$ is observed near 75% Re at each temperature. The interfusion coefficient decreases by a factor of 10 or more as pure Re is approached at each temperature.

- At 1200 °C the mean values for the FCC and HCP phases at the interphase interface are 13.4% Re and 67.0% Re, respectively. At 1350 °C the mean values for the FCC and HCP phases are 16.3% Re and 64.3% Re, respectively.

- No intermediate phase was observed in the diffusion couples.

- Uncertainty limits were established by generating synthetic penetration curves based on the statistics of the deviation of the experimental data from fits. Applying the Sauer-Freise method to these synthetic penetration curves established upper and lower bounds on the diffusion coefficients that were consistent with the variations observed using the initial Sauer-Freise method and the ODE method.

- Broadly speaking, no matter which technique is used there is a relatively large uncertainty associated with the determination of diffusion coefficients from measured solute profiles. Given a measured profile $x_{\mathrm{Re}}(z)$ that exhibits experimental scatter, two equally reasonable fits to within the noise levels can lead to corresponding diffusion coefficients that can differ by as much as a factor of two.

- The raw data can be found at the NIST Materials Repository (http://hdl.handle.net/11256/944).

Appendix 1: The ODE Method

Given an estimate for the diffusion coefficient $\tilde{D}(x_{\mathrm{Re}})$, the ordinary differential equation (ODE) (4) is solved[18,19] by a shooting method. Since the diffusivity is nonlinear and can vary by over an order of magnitude, the ODE is stiff and care must be exercised in the numerical procedure.

Starting from provisional values for $C(\xi_1)$ and its derivative $C'(\xi_1)$ at a given point ξ_1 in the FCC phase, the ODE is integrated to the left hand endpoint $\xi = \xi_L$ and the resulting concentration $C_L = C(\xi_L)$ is recorded. The ODE

is also integrated rightward from ξ_1 until the phase boundary at $\xi = \xi_{\mathrm{phase}}$ is detected, at which point the jump conditions are applied and the integration is resumed until the right hand endpoint is reached at $\xi = \xi_R$. The resulting values of C_L and C_R are then compared to the desired end conditions $c_{\mathrm{Re}}^{\pm}$, and the process is repeated by iterating on the values of $C(\xi_1)$ and $C'(\xi_1)$ until convergence is obtained. A good starting guess is required for $C(\xi_1)$ and $C'(\xi_1)$, and the steps taken by the root solver must be small enough that the ODE solver does not fail via solution blow-up from a bad guess. Suitable starting guesses can be obtained by continuation from a previous solution or an analytical solution for constant $\tilde{D}$.

The resulting composition profiles are compared with the measured profile at the experimental data points, and the least square error between the profiles is used to iterate on $\tilde{D}$ until convergence is obtained. Again it is necessary to control the size of the correction to $\tilde{D}$ in order to avoid blow-up of the ODE solution. In practice, the initial guesses for $\tilde{D}$ can be obtained from a previous solution or an analytical solution, and small trial-and-error changes to $\tilde{D}$ suffice to obtain an approximate solution. An optimization routine[18,19] can then be employed to determine a final solution, again being careful to avoid large steps by the optimizer that can lead to solution blow-up.

The solution to the ODE is smooth in each phase, and the fit to the experimental data generates a least square error that is comparable to that obtained by the purely functional fits used in the Sauer-Freise and UQ methods as shown by Fig. 4 and 5. The error is dominated by the scatter in the experimental data.

The compositions at the phase boundaries are prescribed during this procedure and are not determined self-consistently by the iteration procedure (although the location of the phase boundary itself is an output of the procedure). The reason for prescribing the compositions in advance is that the least square error in the fit is not sensitive to these values once they are given to the precision of the scatter in the data. Instead, provisional values of the phase boundary compositions are determined by visual inspection of the raw data, and the resulting fit to the data is examined in the locality of the phase boundary. Small changes to the prescribed phase boundary compositions that improve the local fit are then applied, and the overall procedure is repeated. The possible ranges of the phase boundary compositions that do not change the least square error can be taken as a measure of their uncertainty.

Finally, there is an additional complication that is particular to the two-phase problem. If the current numerical solution computes an interface location that is one or more mesh points distant from the location indicated by the

762

J. Phase Equilib. Diffus. (2017) 38:750–763

experimental data, there is an associated local error in the fit that is of order unity. On the other hand, if the computed and experimental phase boundaries occur at the same mesh point, this component of the error can be significantly smaller. The computed interface position is most sensitive to the value of the Matano position z_0, but also depends on the diffusion parameters A_j and B_j. As an optimizer scans parameter space in search of an accurate fit, the computed error in the fit can appear to change discontinuously as the numerical solution goes into and out of alignment with the experimental position of the phase boundary, which can significantly interfere with the optimizer's smoothness assumptions. It is primarily this feature of the two-phase couple that prevents the success of an automated global optimization approach for the ODE method for this two phase diffusion couple.

Appendix 2: The UQ Method

In the uncertainty quantification and machine learning communities, Gaussian-processes (GPs) are well known tools for modeling noise and uncertainty in data. As there are many references that provide comprehensive reviews of the subject, we only introduce the main ideas and highlight issues that are relevant for constructing synthetic datasets.[17,20,21]

To begin, let $\mathbf{z} = (z_1, \ldots, z_N)$ be a vector of the N positions at which we know the residuals $\mathbf{r}(\mathbf{z}) = (r(z_1), \ldots, r(z_N))$; see Fig. 4 and 5. The starting point of our analysis is to assume that the $\mathbf{r}(\mathbf{z})$ are sampled from a Gaussian stochastic process, i.e. a random function whose joint probabilities between finitely many values are multivariate Gaussian random variables. Mathematically, this means that the probability density of the residuals taking values $\mathbf{r}$ at positions $\mathbf{z}$ is given by

$$P[\mathbf{r}(\mathbf{z})] = \frac{1}{(2\pi)^{N/2} |K(\mathbf{z}, \mathbf{z})|} \exp\left\{ \frac{-1}{2} \mathbf{r}^T K(\mathbf{z}, \mathbf{z})^{-1} \mathbf{r} \right\},$$
(Eq A1)

where $K(\mathbf{z}, \mathbf{z})$ is defined as

$$K(\mathbf{z}, \mathbf{z}) = \begin{bmatrix} K(z_1, z_1) & \cdots & K(z_1, z_N) \\ \vdots & \ddots & \vdots \\ K(z_N, z_1) & \cdots & K(z_N, z_N) \end{bmatrix}.$$
(Eq A2)

$K(z_i, z_j)$ is a covariance matrix element indicating the extent to which the residual at z_i is correlated with the residual at z_j, and $|K(\mathbf{z}, \mathbf{z})|$ is the determinant of $K(\mathbf{z}, \mathbf{z})$. The goal of our noise modeling is to use the experimental residuals to determine the function K.

Now, it is generally impossible for data to effect a regression by itself; we must invoke some additional or outside information. In the case of GP modeling, one postulates a functional form of the covariance K, parameterized by some unknown set of constants φ. The constants are often referred to as hyperparameters. For all of the regression in this work, we use the Matérn covariance function

$$K(z_i, z_j; \sigma, v, \rho) = \sigma^2 \frac{2^{1-v}}{\Gamma(v)} \left(\sqrt{2v} \frac{|z_i - z_j|}{\rho} \right)^v \kappa_v \left(\sqrt{2v} \frac{|z_i - z_j|}{\rho} \right),$$
(Eq A3)

where κ_v is the modified Bessel function of the second kind of order v, Γ is the gamma function, σ is the amplitude of the noise, and ρ is a length specifying the characteristic distance over which residuals are correlated. Here we identify the free parameters as $\varphi = (\sigma, v, \rho)$. Notably, this covariance is sometimes recommended for spatial data that may not be very smooth,[22] as is the case with our data, especially on the Re-rich HCP side of the diffusion couple.

To generate synthetic data, we first determine the set φ via a maximum likelihood analysis. Specifically, we insert $K(\mathbf{z}, \mathbf{z})$ in Eq A1 and maximize the probability our residuals as a function of these three parameters; that is, we determine the set of φ that is most likely to reproduce our experimental residuals. This computation can be done using canned routines in, e.g. Matlab. Given these parameters, we then compute the Cholesky decomposition (i.e. matrix square root) L such that $K(\mathbf{z}, \mathbf{z}) = LL^T$. Using a random number generator, one requests N independent, identically distributed Gaussian random variables with unit variance. Denoting the jth realization as a vector $\mathbf{H}^j$, we then compute the jth realization of synthetic residuals as the matrix product $\boldsymbol{\eta}^j = L \, \mathbf{H}^j$ for $\boldsymbol{\eta}^j = (\eta^j(z_1, \varphi), \eta^j(z_2, \varphi), \ldots)$ appearing in Eq 15. Repeating this process with new random numbers generates different synthetic residuals.[17]

Given that the FCC and HCP phases generally exhibit different residuals, we use the functions $f(z)$ and $h(z)$ (cf. Eq 13) to construct separate noise models associated with each phase. Then, we generate a full synthetic dataset by combining one realization from both models. This full dataset is subsequently analyzed using the procedure described above in the section, Assessment of $\tilde{D}$ and uncertainty using a statistical method.

References

1. K. Yaqoob and J.-M. Joubert, Experimental Determination and Thermodynamic Modeling of the Ni-Re Binary System, *J. Solid State Chem.*, 2012, **196**, p 320-325
2. S. Saito, T. Takashima, K. Miyama, K. Kurokawa, and T. Narita, Tie-Line Compositions of the γ and γ' Phases in the Binary Re-Ni System, *Mater. Trans.*, 2012, **53**, p 1078-1083

3. S.B. Maisel, N. Schindzielorz, A. Mottura, R.C. Reed, and S. Müller, Nickel-Rhenium Compound Sheds Light on the Potency of Rhenium as a Strengthener in High-Temperature Nickel Alloys, *Phys. Rev. B*, 2014, **90**, p 094110

4. C.M. Neubauer, D. Mari, and D.C. Dunand, Diffusion in the Ni-Re System, *Scr. Metall. Mater.*, 1994, **31**, p 99-104

5. M.S.A. Karunaratne, P. Carter, and R.C. Reed, Interdiffusion in the Face-Centered Cubic Phase of the Ni-Re, Ni-Ta and Ni-W Systems Between 900 and 1300 °C, *Mat. Sci. Eng.*, 2000, **A281**, p 229-233

6. G. Neumann and C. Tuijn, *Self-Diffusion and Impurity Diffusion in Pure Metals*, Elsevier, Amsterdam, 2009, p 283 (Table 8.2)

7. Q. Zeng, S.W. Ma, Y.R. Zheng, S.Z. Liu, and T. Zhai, A study of Re and Al Diffusion in Ni, *J. Alloys Compd.*, 2009, **480**, p 987-990

8. R.A. Hobbs, M.S.A. Karunaratne, S. Tina, and R.C. Reed, Uphill Diffusion in Ternary Ni-Re-Ru Alloys at 1000 and 1100 °C, *Mater. Sci. Eng. A*, 2007, **460-461**, p 587-594

9. A.I. Epishina, A.O. Rodin, B.S. Bokshtein, G. Oder, T. Link, and I.L. Svetlov, Interdiffusion in Binary Ni–Re Alloys, *Phys. Met. Metallogr.*, 2015, **116**, p 175-181

10. C.S. Barrett and T.B. Massalski, *Structure of Metals*, 3rd ed., McGraw-Hill, New York, 1966 (Table A-6 (converted from volume/atom to volume/mole of atoms))

11. G.S. Hartley and J. Crank, *Trans. Faraday Soc.*, 1946, **B42**, p 123

12. R.W. Balluffi, On the Determination of Diffusion Coefficients in Chemical Diffusion, *Acta Metall.*, 1960, **8**, p 871-873

13. R.F. Sekerka, G.B. McFadden, and W.J. Boettinger, Analytical Derivation of the Sauer-Freise Flux Equation for Multicomponent Multiphase Diffusion Couples with Variable Partial Molar Volumes, *J. Phase Equilib. Diffus.*, 2016, **37**, p 640-650

14. J.E. Reynolds, B.L. Averbach, and M. Cohen, Self-Diffusion and Interdiffusion in Gold-Nickel Alloys, *Acta Metall.*, 1957, **5**, p 29-40

15. M.J.H. van Dal, M.C.L.P. Pleumeekers, A.A. Kodentsov, and F.J.J. van Loo, Diffusion Studies and Re-Examination of the Kirkendall Effect in the Au-Ni System, *J. Alloys Compd.*, 2000, **309**, p 132-140

16. R. Bouchet and R. Mevrel, A Numerical Inverse Method for Calculating the Interdiffusion Coefficients Along a Diffusion Path in Ternary Systems, *Acta Mater.*, 2002, **50**, p 4887-4900

17. C.E. Rasmussen and C.K.I. Williams, *Gaussian Processes for Machine Learning (Adaptive Computation and Machine Learning)*, MIT Press, Cambridge, 2005

18. D. Kahaner, C. Moler, and S. Nash, *Numerical Methods and Software*, PrenticeHall, Englewood Cliffs, 1989

19. Bill Buzbee, *The SLATEC Common Math Library, in Sources and Development of Mathematical Software, edited by Wayne Cowell*, Prentice-Hall, Englewood Cliffs, 1984

20. T.J. Santner, B. Williams, and W. Notz, *The Design and Analysis of Computer Experiments*, Springer, New York, 2003

21. J. Sacks, W.J. Welch, T.J. Mitchell, and H.P. Wynn, *Stat. Sci.*, 1989, **4**, p 409

22. M.L. Stein, *Interpolation of Spatial Data: Some Theory for Kriging*, Springer, New York, 1999